FINITE-STATE DYNAMIC WAKE INFLOW MODELLING FOR COAXIAL ROTORS

Felice Cardito, Riccardo Gori, Giovanni Bernardini,
Jacopo Serafini, Massimo Gennaretti

Department of Engineering, Roma Tre University, Rome, Italy

Abstract

Wake inflow modelling is a crucial issue in the development of efficient and reliable computational tools for flight mechanic and aeroelastic analysis of rotorcraft. The aim of this work is the development of a finite-state, dynamic wake inflow modelling for coaxial rotors in steady flight conditions, based on simulations provided by aerodynamic solvers of arbitrary accuracy. It provides models relating the coefficients of an approximated linear distribution of wake inflow over upper and lower rotor discs either to rotor controls and helicopter kinematic variables or to thrust and in-plane moments generated by the rotors. A three-step identification procedure is proposed. It consists in: (i) evaluation of wake inflow due to harmonic perturbations of rotor kinematics, (ii) determination of the corresponding inflow coefficient (and rotor loads) transfer functions, and (iii) their rational approximation. Wake inflow models are predicted through aerodynamic solutions provided by a boundary element method for potential flows, capable of capturing effects due to wake distortion, multi-body interference (like that in coaxial rotor configurations) and severe blade-vortex interaction. They are validated by correlation with the inflow directly calculated by the aerodynamic solver, for a coaxial rotor system subject to arbitrary perturbations.

1. INTRODUCTION

The aim of this work is the development of a finite-state model for the prediction of perturbation dynamic wake inflow over coaxial rotors in arbitrary steady motion.

Because of the improved performance they may provide, coaxial rotors are expected to become an efficient solution for next-generation rotorcraft. Indeed, as the forward flight speed increases, the difference of dynamic pressure between the advancing and retreating sides of a single rotor becomes greater. This requires higher values of the cyclic pitch both to maintain the aircraft in roll trim, and to tilt the disk further forward to overcome the helicopter drag increase. In order to avoid blade stall on the retreating side of the rotor disk, the amount of collective pitch has to be correspondingly reduced, thus negatively affecting the rotor thrust capability, and leaving rotor designers in a speed trap.[1] In coaxial, counter-rotating rotor configurations (as those proposed, for instance, in the Advancing Blade Concept -ABC- research helicopter introduced by the Sikorsky Aircraft in the sixties) the advancing blades of each rotor may operate at higher pitch angles to produce more lift without prejudice to roll trim, since the difference in lift between the advancing and retreating sides of the upper rotor is balanced by the opposite one arising on the lower rotor (indeed, the concept derives its name from the fact that it makes more efficient use of the lift generated on the advancing blades at high speed forward flight). Then, rotor lift is retained with increasing speed and speed capability is maintained at altitude.[2] In addition, the maximum lift-to-drag ratio is improved. In terms of induced power consumption, the coaxial rotors have proven to be intrinsically more efficient in hover, forward flight and during manoeuvres than single rotors of the same solidity and blade geometry.[3] ABC provides not only performance benefits, but also satisfactory handling qualities, loads and dynamics.[2] Furthermore, coaxial rotors provide torque cancellation, thereby eliminating the need for a tail rotor and its associated shafting and gearboxes.

All this motivates the development of computational tools suitable for analysis and design of coaxial rotors. Dynamic wake inflow modeling is one of the main issues in efficient and reliable rotorcraft simulation tools concerning aeroelasticity, flight mechanics, and handling quality assessment, as well as for flight control laws definition (see, for instance, Refs. [4, 5]).

This paper proposes the development of linear, time-invariant, finite-state modelling for the prediction of perturbation rotor dynamic wake inflow over coaxial rotors,

based on simulations provided by aerodynamic solvers of arbitrary accuracy. Inspired by the well-known Pitt-Peters dynamic inflow model,[6,7] it is derived through an identification process technique similar to that introduced in the past for rotary-wing aerodynamics and aeroelasticity finite-state modeling,[8,9] and extends to coaxial rotors the methodology recently presented for isolated rotors.[10] Two types of wake inflow models are presented: the first one directly related to the helicopter flight dynamics variables (namely, state-space and blade control variables), and the second one related to rotor loads (as in the Pitt-Peters model). They are both based on rotor aerodynamics simulations provided by a Boundary Element Method (BEM) tool for the solution of a boundary integral equation formulation for the velocity potential field around rotors in arbitrary motion.[11] This aerodynamic solver is capable of taking into account wake distortion and multi-body interference effects (like those present in coaxial rotors or rotor-fuselage systems), as well as of simulating severe blade-vortex interaction (BVI) events. A time-marching aerodynamics solution scheme is applied to identify transfer functions relating perturbation motion with wake inflow and rotor loads, and then the finite-state modelling is obtained through a rational-matrix approximation algorithm developed by some of the authors.[8,9] It is worth observing that, the proposed wake inflow modelling approach may be applied in combination with any rotor aerodynamics solver, of arbitrary accuracy and complexity. Coupled with sectional aerodynamic load theories, the resulting models may be conveniently applied for rotor aeroelastic modelling in flight dynamics stability and control applications.

The numerical investigation examines the accuracy of the transfer function identification and rational approximation processes, and presents the validation of the proposed dynamic inflow models by comparison with the wake inflow directly calculated by the time-marching BEM solver, for coaxial rotor configurations in steady flight, subject to arbitrary perturbations.

2. COAXIAL ROTOR WAKE-INFLOW MODELLING

A novel wake inflow perturbation modelling extending to coaxial rotors the methodology proposed in Ref. [10] for single rotors is presented in this section.

Akin to the model introduced in Refs. [6,7], the distributions of wake inflow perturbation, $\lambda_i^{u,l}$, over the upper and lower rotor discs are approximated by the following linear interpolation formulas, each defined in a non-rotating polar coordinate system, (r, ψ),

$$
(1) \quad \begin{aligned} \lambda_i^{u,l}(r,\psi,t) &= \lambda_0^{u,l}(t) \\ &+ r\left[\lambda_s^{u,l}(t)\sin\psi + \lambda_c^{u,l}(t)\cos\psi\right] \end{aligned}
$$

where r denotes distance from the disc centre, ψ is the azimuth distance from the rear blade position, while $\lambda_0^{u,l}$, $\lambda_s^{u,l}$ and $\lambda_c^{u,l}$ represent, respectively, instantaneous mean value, side-to-side gradient and fore-to-aft gradient on the upper and lower rotor disc. The objective is to derive a linear, time-invariant (LTI), finite-state wake inflow differential operator, relating these wake inflow components to flight dynamics state variables and controls, or rotor loads.

The novel model identification methodology proposed consists in a multi-step process, starting with the evaluation of the transfer functions relating wake inflow components, $\boldsymbol{\lambda}_i = \left\{\lambda_0^u \; \lambda_s^u \; \lambda_c^u \; \lambda_0^l \; \lambda_s^l \; \lambda_c^l\right\}^T$, to perturbations of hub motion given in terms of linear and angular velocity components, $\mathbf{q}_h = \{u \; v \; w \; p \; q \; r\}^T$, and blade pitch controls on upper and lower rotors, $\mathbf{q}_\theta = \{\theta_0^- \; \theta_s^- \; \theta_c^- \; \theta_0^+ \; \theta_s^+ \; \theta_c^+\}^T$ (where, for instance, $\theta_0^+ = (\theta_0^u + \theta_0^l)/2$ and $\theta_0^- = (\theta_0^u - \theta_0^l)/2$), about a steady, trimmed flight condition. This is accomplished by an arbitrary aerodynamic solver, whose level of accuracy determines the level of accuracy of the resulting wake inflow model. In this paper, a free-wake aerodynamic BEM solver for potential flows around lifting rotors is used. It is applicable to any rotorcraft configuration, with inclusion of coaxial rotors, where mutual interference effects may play a crucial role.[11]

For $\lambda_B^{u,l}(r,\psi,t)$ denoting the wake inflow perturbation computed on upper and lower rotor blades located at the azimuthal position, ψ, at time, t, the wake inflow components, $\lambda_0^{u,l}$, $\lambda_s^{u,l}$ and $\lambda_c^{u,l}$, are determined as those that minimize the two error quadratic indeces, $J^{u,l}$, i.e., those yielding

$$
J^{u,l}(t) = \int_{r_c}^{R} \sum_{i=1}^{N_b}\left[\lambda_B^{u,l}(r,\psi_i,t) - \lambda_i^{u,l}(r,\psi_i,t)\right]^2 \mathrm{d}r = \min
$$

$\forall t$, where R and r_c are upper and lower rotor radius and blade aerodynamic root cut-off, respectively, while N_b is the number of rotor blades (for the sake of simplicity, and with no loss of generality of the proposed formulation, N_b, R and r_c on upper and lower rotor have been assumed to be equal). Thus, at a given time, t, the imposition of $\partial J^{u,l}/\partial\lambda_0^{u,l} = 0$, $\partial J^{u,l}/\partial\lambda_s^{u,l} = 0$ and

$\partial J^{u,l}/\partial \lambda_c^{u,l} = 0$ provides

$$\lambda_0^{u,l}(t) = \frac{1}{(R - r_c)} \frac{1}{N_b} \sum_{i=1}^{N_b} \int_{r_c}^{R} \lambda_{\scriptscriptstyle B}(r, \psi_i, t)\, \mathrm{d}r$$

$$\lambda_s^{u,l}(t) = \frac{3}{(R^3 - r_c^3)} \frac{1}{N_b/2} \sum_{i=1}^{N_b} \int_{r_c}^{R} \lambda_{\scriptscriptstyle B}(r, \psi_i, t)\, \sin\psi_i\, r\, \mathrm{d}r$$

$$\lambda_c^{u,l}(t) = \frac{3}{(R^3 - r_c^3)} \frac{1}{N_b/2} \sum_{i=1}^{N_b} \int_{r_c}^{R} \lambda_{\scriptscriptstyle B}(r, \psi_i, t)\, \cos\psi_i\, r\, \mathrm{d}r$$

Following an approach similar to that recently presented for single rotor wake inflow modelling,[10] the identification of the transfer function matrices, $\mathbf{H}_h$ and $\mathbf{H}_\theta$, relating the Fourier transform of wake inflow components to the Fourier transform of hub motion and pitch control, *i.e.,* such that

(2) $\tilde{\boldsymbol{\lambda}}_i = \mathbf{H}_h\, \tilde{\mathbf{q}}_h + \mathbf{H}_\theta\, \tilde{\mathbf{q}}_\theta = \mathbf{H}\, \tilde{\mathbf{q}}$

with $\mathbf{q} = \left\{ \mathbf{q}_h^T\ \mathbf{q}_\theta^T \right\}^T$ and $\mathbf{H} = [\mathbf{H}_h\ \mathbf{H}_\theta]$, is achieved in the following way:

(i) a time-marching aerodynamic solver is applied to evaluate wake inflow perturbations generated by small, single-harmonic perturbations of each element of vector $\mathbf{q}$;

(ii) the harmonic components of the resulting wake inflow components having the same frequency of the input are extracted and then, the corresponding complex values of the frequency-response functions are determined;

(iii) the process is repeated for a discrete number of frequencies within an appropriate range, so as to get an adequate sampling of the frequency-response functions appearing in $\mathbf{H}$.

Note that, extracting from the output only the component having the same harmonic of the input implies that a linearized, constant-coefficient approximation of the operator relating $\boldsymbol{\lambda}_i$ to $\mathbf{q}$ is pursued (the aerodynamic operator concerning rotors in forward flight is intrinsically non-linear with periodic-coefficients and, as such, multi-harmonic outputs correspond to single-harmonic inputs).[12,13]

It is worth mentioning that the harmonic wake inflow components are obtained through a discrete Fourier transform algorithm, taking care of the following issues:[12,13]

- the wake inflow response is examined after the transient is vanished;

- the period examined is an integer multiple of the period of the input signal;

- almost periodic responses might arise because of the intrinsic periodicity of the aerodynamic operator, (unless a hovering condition is examined) thus leakage is made negligible considering a period of response that is long enough (alternatively, suitable windowing may be applied).

The final steps in the process of identification of the finite-state representation of the rotor wake inflow consist in deriving rational forms (*i.e.,* with a finite number of poles) that provide the best fit to the transfer functions sampled in the frequency domain, followed by transformation into time domain. Specifically, from the application of a least-square procedure assuring the stability of the identified poles, the transfer-function matrix, $\mathbf{H}$, is approximated by the rational-matrix approximation form (RMA)[13,14]

(3) $\mathbf{H}(s) \approx s\, \mathbf{A}_1 + \mathbf{A}_0 + \mathbf{C}\, [s\, \mathbf{I} - \mathbf{A}]^{-1}\, \mathbf{B}$

where $\mathbf{A}_1, \mathbf{A}_0, \mathbf{A}, \mathbf{B}$ and $\mathbf{C}$ are real, fully populated matrices, while s denotes the Laplace-domain variable. Matrices $\mathbf{A}_1$ and $\mathbf{A}_0$ have dimensions $[6 \times 12]$, $\mathbf{A}$ is a $[N_a \times N_a]$ matrix containing the N_a poles of the rational expression, $\mathbf{B}$ is a $[N_a \times 12]$ matrix, and $\mathbf{C}$ has dimensions $[6 \times N_a]$.

Then, transforming Eq. 3 into time domain yields the following finite-state dynamic wake inflow model

(4) $\begin{aligned} \boldsymbol{\lambda}_i(t) &= \mathbf{A}_1\, \dot{\mathbf{q}}(t) + \mathbf{A}_0\, \mathbf{q}(t) + \mathbf{C}\, \mathbf{r}(t) \\ \dot{\mathbf{r}}(t) &= \mathbf{A}\, \mathbf{r}(t) + \mathbf{B}\, \mathbf{q}(t) \end{aligned}$

where $\mathbf{r}$ are the additional states representing wake inflow dynamics. This model is capable of taking into account all aerodynamic phenomena simulated by the aerodynamic solver applied for the transfer function sampling.

Coupling Eq. 1 with Eq. 4 provides the time history of the wake inflow linear distributions on upper and lower rotor discs, as associated to arbitrary hub motion and pitch control perturbations.

2.1. Pitt-Peters-type wake inflow modelling

Starting from the model present above, an alternative Pitt-Peters-type dynamic inflow model relating the components of the inflow linear approximation to rotor loads

(instead of hub motion and pitch controls) is proposed, as well. It requires the additional evaluation, through the same aerodynamic solver applied for the wake inflow determination, of the transfer function matrix between the kinematic input variables ($\mathbf{q}_h$ or $\mathbf{q}_\theta$) and thrust, roll moment and pitch moment generated by upper and lower rotors, $\mathbf{f} = \{C_T^u \, C_L^u \, C_M^u \, C_T^l \, C_L^l \, C_M^l\}^T$ (it is worth noting that these rotor loads are linearly related to blade bound circulation, and hence to the corresponding wake vorticity and inflow; the remaining three rotor loads -namely, lateral forces and torque- are closely related to induced drag and hence quadratically related to inflow). From each set of kinematic variables a different Pitt-Peters-type dynamic inflow model is derived.

Considering the perturbations of the kinematic variables, $\mathbf{q}_h$, the first step of the alternative model derivation consists in evaluating the transfer matrix, $\mathbf{G}_h$, such that $\tilde{\mathbf{f}} = \mathbf{G}_h \, \tilde{\mathbf{q}}_h$ through a procedure similar to that applied for Eq. 2 (*i.e.,* by replacing the aerodynamic output $\boldsymbol{\lambda}_i$ with $\mathbf{f}$).

Then, for each sampling frequency, the inverse of matrix $\mathbf{G}_h$ is determined and the wake inflow components are directly related to the rotor loads by the expression

(5) $\tilde{\boldsymbol{\lambda}}_i = \hat{\mathbf{H}}_h \, \tilde{\mathbf{f}}$

where $\hat{\mathbf{H}}_h = \mathbf{H}_h \mathbf{G}_h^{-1}$ is the $[6 \times 6]$ transfer function matrix.

Finally, the RMA of the frequency distribution of $\hat{\mathbf{H}}_h$,

(6) $\hat{\mathbf{H}}_h(s) = \mathbf{A}_0 + \mathbf{C}\,(s\mathbf{I} - \mathbf{A})^{-1}\,\mathbf{B}$

with $[\mathbf{A}_0] = [6 \times 6]$, $[\mathbf{A}] = [N_a \times N_a]$, $[\mathbf{B}] = [N_a \times 6]$ and $[\mathbf{C}] = [6 \times N_a]$, followed by transformation into time domain yields the LTI, finite-state, Pitt-Peters-type dynamic wake inflow model that reads

(7)
$$\boldsymbol{\lambda}_i(t) = \mathbf{A}_0 \, \mathbf{f}(t) + \mathbf{C} \, \mathbf{r}(t)$$
$$\dot{\mathbf{r}}(t) = \mathbf{A} \, \mathbf{r}(t) + \mathbf{B} \, \mathbf{f}(t)$$

In this case $\mathbf{A}_1$ has been neglected in that it is expected that the wake vorticity and the corresponding wake inflow are related to rotor loads, but not to their time derivatives.

Repeating the process with $\mathbf{q}_\theta$ perturbations replacing the $\mathbf{q}_h$ perturbations, first the matrix $\mathbf{G}_\theta$, such that $\tilde{\mathbf{f}} = \mathbf{G}_\theta \, \tilde{\mathbf{q}}_\theta$ might be computed, and then derivation and RMA of the Pitt-Peters-type transfer function matrix, $\hat{\mathbf{H}}_\theta$, such that $\hat{\mathbf{H}}_\theta = \mathbf{H}_\theta \mathbf{G}_\theta^{-1}$, would provide an equivalent (but different) LTI, finite-state, Pitt-Peters-type dynamic wake inflow model.

Coupling Eq. 1 with Eq. 7 provides the time history of the wake inflow linear distributions on upper and lower rotor discs, as associated to rotor loads.

3. NUMERICAL RESULTS

In this section, the proposed finite-state wake inflow modelling is verified and validated by application of the aerodynamic solution provided by an unsteady, potential-flow, BEM tool for rotorcraft, extensively validated in the past[11, 15, 16]

For a coaxial rotor system composed of two idential three-bladed rotors, having radius $R = 5.48$ m, blade root chord $c = 0.54$ m, taper ratio $\lambda = 0.5$, twist $\theta_{tw} = -7°$, and counter-rotating at angular velocity $\Omega = 32.8$ rad/s, both the wake inflow modeling based on kinematic perturbations and the Pitt-Peters-type model (*i.e.,* based on rotor loads) are analyzed. Specifically, wake inflow transfer functions and their rational approximation are examined, along with the capability of the resulting finite-state model to predict wake inflows due to arbitrary rotor perturbations. In addition, for the Pitt-Peters-type model, the influence of the type of kinematic perturbations used for its identification is discussed.

The rotor wake in the aerodynamic BEM solver is assumed to have a prescribed shape that, in forward flight, coincides with the surface swept by the trailing edges, whereas in hovering condition consists of a helicoidal surface with spiral length given by the mean inflow of the trimmed operative condition. The importance of a more realistic wake shape provided by a free-wake aerodynamic solution algorithm has already been pointed out in Ref. [10] for single rotors. However, since the purposes of the paper are the presentation and the assessment of feasibility and features of a novel approach for the development of finite-state wake inflow modelling for coaxial rotors, these would not be significantly affected by the wake model applied in the aerodynamic simulations.

3.1. Approximated representation of wake inflow

First, considering the case of the rotor in hovering condition, the accuracy of the inflow representation applied here (see Eq. 1) is analysed. Note that, for symmetry reasons, the mean inflow components, λ_0, depends only on axi-symmetric perturbations, whereas λ_s and λ_c are perturbed only by non axi-symmetric inputs.

Figure 1(a) shows the computed wake inflow radial distributions, $\lambda_B^{+,-}$, caused by stationary perturbations of θ_0^+ and θ_0^- (namely, blade and differential collec-

(a) λ_B due to θ_0.

(b) λ_B due to θ_s.
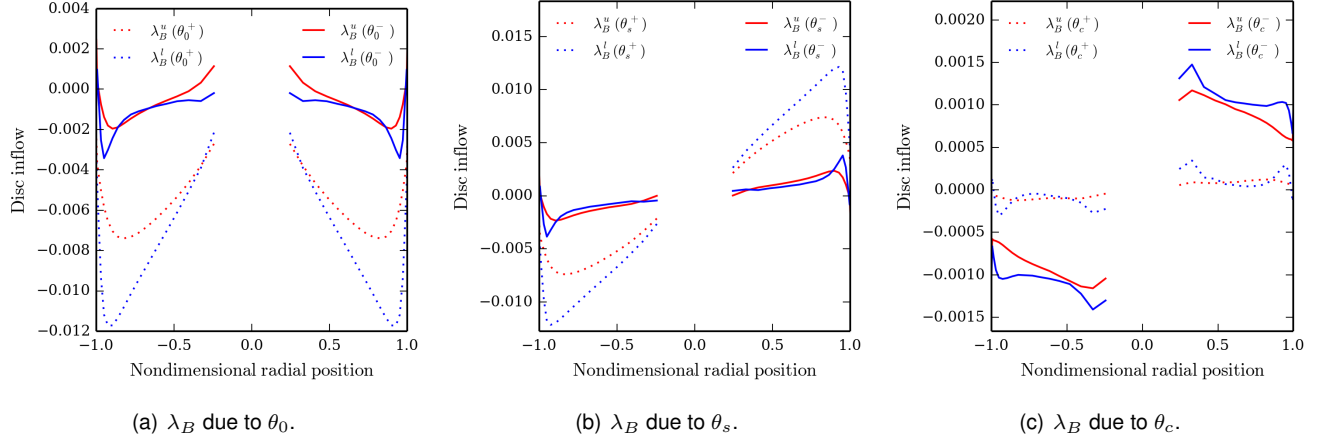
(c) λ_B due to θ_c.

Figure 1: Wake inflow distribution on blades at $\psi = \pi/2$ (right) and $\psi = 3\pi/2$ (left).

tive pitches, respectively), evaluated on the blade when passing at azimuth locations $\psi = \pi/2$ (right) and $\psi = 3\pi/2$ (left). As already shown in Ref. [10], it is evident that the inflow representation applied can only provide a rough approximation of the perturbed inflow distribution. Indeed, in symmetric cases, it consists of a constant value, λ_0, which is quite far from the wake inflow radial distributions in Fig. 1(a).

Furthermore, Figs. 1(b) and 1(c) present the computed wake inflow due to (non-axi-symmetric) perturbations of blade and differential longitudinal and lateral pitches (namely, $\theta_c^{+,-}$ and $\theta_s^{+,-}$). Also in these cases, the approximations consisting of linear radial distributions are, especially at the blade tips, quite far from the computed values. This is particularly true for the responses to the differential perturbation, θ_c^-. Comparing Figs. 1(b) and 1(c), it is worth noting that, unlike the single rotor case, where the wake inflow response to θ_c tends to be negligible on blades passing at $\psi = \pi/2$ and $\psi = 3\pi/2$, differential perturbations on θ_c produce inflow perturbations comparable with those generated by differential perturbations on θ_s, thus denoting remarkable coupling occurring in coaxial rotors between the harmonic components of inflow and blade pitch controls.

These observations are confirmed by Fig. 2, that shows wake inflow distributions on a rotor blade during one revolution, induced by stationary blade pitch perturbations. In Figs. 2(a)-2(d), the inflows on the upper and lower rotors caused by an axi-symmetric perturbation present both azimuthal 6/rev-period harmonic behavior and radial gradients that cannot be captured by the representation in Eq. 1. This points out the need to develop a more complex approximation of the wake inflow, capable to take into account higher-order radial dis-

tributions and higher-harmonic azimuthal distributions. Similar conclusions are drawn from Figs. 2(c) and 2(d) depicting upper and lower disc distributions of wake inflow induced on rotor blades by (non-axisymmetric) differential lateral pitch perturbations. In this case, the disc inflow presents a directivity aligned about with the $\psi = 150$ deg direction, while it is closely aligned with the $\psi = 180$ deg direction in a single rotor system.

In forward flight conditions, it is expected that the mathematical model in Eq. 1 is even less suitable for representing coaxial rotor wake inflow. Indeed, for an advance ratio $\mu = 0.2$, Fig. 3 shows the complexity of the inflow distribution due to the same perturbations considered in Fig. 2. In this case, the azimuthal 6/rev-period harmonic behavior is hidden by the superimposed 1/rev effect of the wake spatial development along the direction of motion. However, very complex radial distributions are combined with higher-harmonic azimuthal distributions that cannot be accurately captured by Eq. 1.

Despite the observations concerning the accuracy of wake inflow representations based on Eq. 1, it is important to remind that the suitability of wake inflow approximations is strictly related to the applications they are addressed to. For instance, it is well known that, although not providing a detailed representation of the wake inflow, Eq. 1 is suited for flight dynamics applications involving low-frequency rotor aeroelastic simulations.
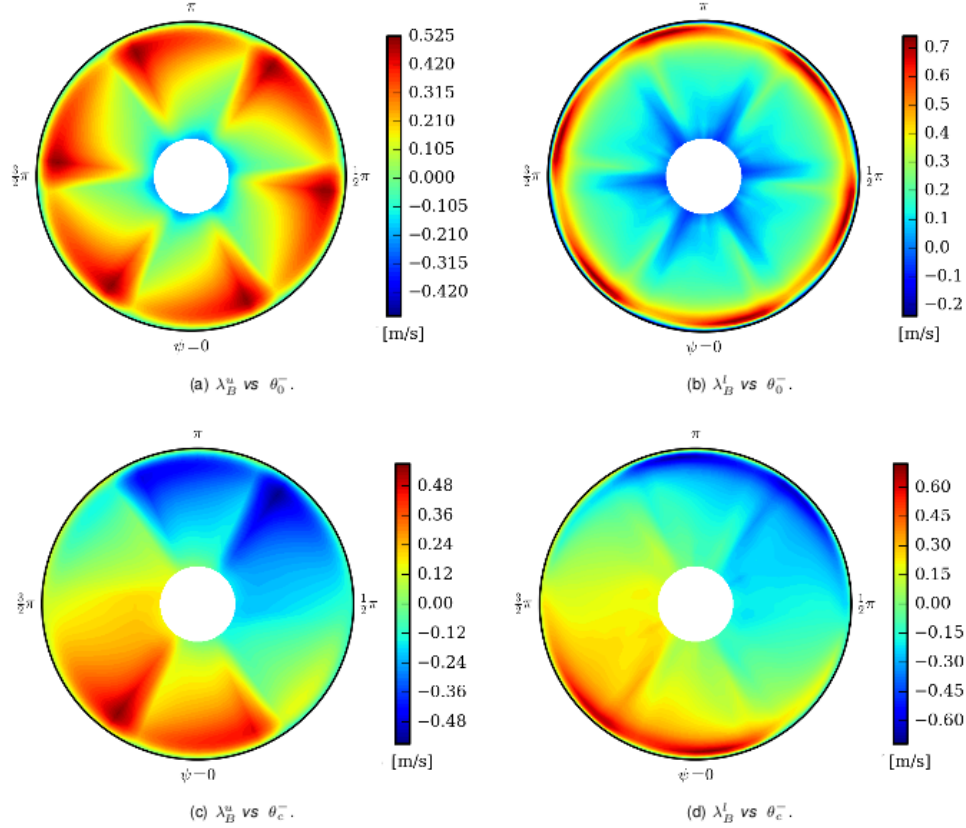
Figure 2: Wake inflow distribution over rotor discs. Hovering condition.

3.2. Transfer functions for hovering rotor and corresponding RMA: pitch control/kinematics perturbations

Next, the transfer functions relating $\boldsymbol{\lambda}_i$ to $\mathbf{q}_\theta$ identified through the procedure explained in Section 2, and their RMA are discussed for the rotor in hovering condition. Figure 4 shows a subset of the elements of the 6×6 transfer functions matrix, $\mathbf{H}_\theta$, with the remaining ones that are either negligible or identical to those shown, for symmetry reasons. The wake inflow components on the two rotors present remarkable differences: on the lower rotor, their transfer functions are generally of higher amplitude than upper rotor's ones, particularly those concerning blade pitch components, $\theta_0^+, \theta_c^+, \theta_s^+$, and tends to have a slower decay with frequency increase, thus revealing the presence of high-frequency poles (see Figs. 4(a), 4(c) and 4(f)).

For all of the transfer functions included in the matrix $\mathbf{H}_\theta$, the RMA is achieved by introduction of ten poles (*i.e.,* ten additional aerodynamic states), and appears in excellent agreement with their sampled values.

Similarly, identified transfer functions relating $\boldsymbol{\lambda}_i$ to $\mathbf{q}_h$ are shown in Fig. 5, using the same selection criterion adopted for Fig. 4. The comments to Fig. 4 concerning the difference of amplitude and high-frequency behaviour between upper rotor and lower rotor wake inflow transfer functions are generally still valid, with partial exceptions represented by the results in Fig. 5(c) where the amplitude of the upper rotor transfer function is significantly higher in the lower-frequency range than that of the lower rotor, and in Fig. 5(f) where high-frequency poles are present in the upper rotor transfer function, as well.

It is interesting to note the similarity between the transfer funtions λ_s *vs* θ_s^+ and λ_s *vs* p (see Figs. 4(f) and 5(e)), as well as that between λ_s *vs* θ_c^+ and λ_s *vs* q (see Figs. 4(d) and 5(f)): these are consistent with the similarity between the blade kinematic effects (and consequent release of wake vorticity) produced by perturbations of θ_s^+ and p and by perturbations of θ_c^+ and q.
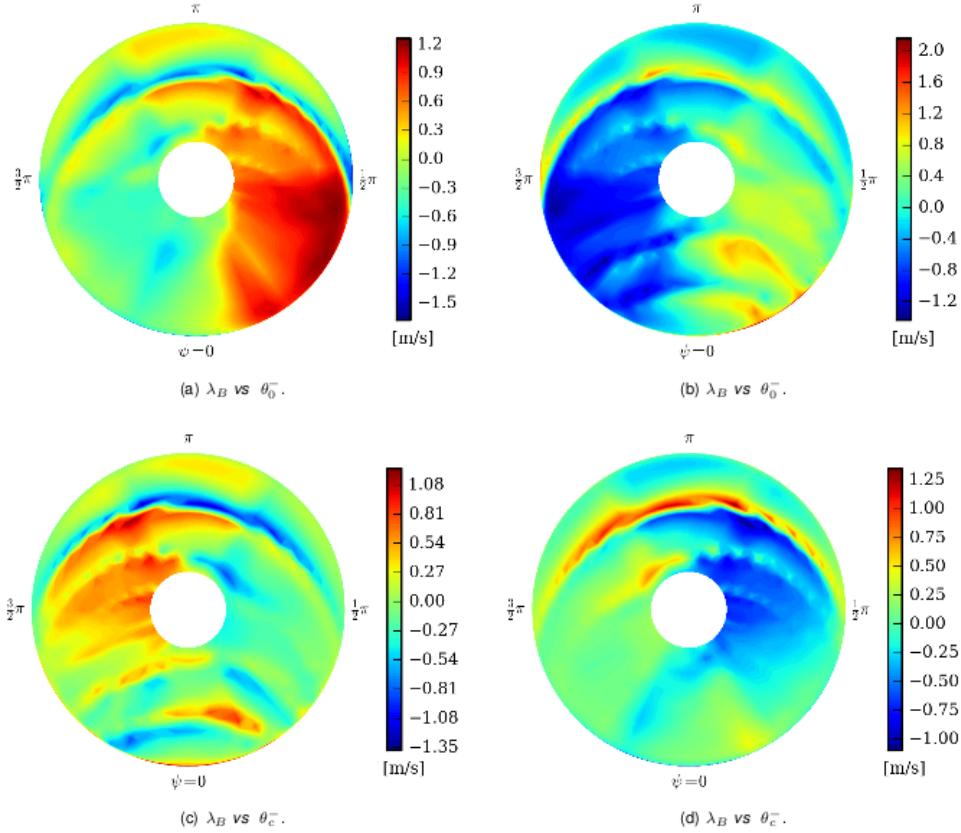
Figure 3: Wake inflow distribution over rotor discs. Forward flight condition.

3.3. Transfer functions of Pitt-Peters-type inflow model for hovering rotor

Starting from the wake inflow transfer functions concerning blade control pitch and kinematic perturbations, Pitt-Peters-type wake inflow models are identified following the methodology outlined in Section 2.1., for the hovering rotor condition. Specifically, taking advantage of the knowledge of $\mathbf{H}_h$ and $\mathbf{H}_\theta$, the transfer function matrices $\hat{\mathbf{H}}_h$ and $\hat{\mathbf{H}}_\theta$ are derived (see Section 2.1.).

Figure 6 shows numerically sampled values and RMA of the most significant transfer functions in $\hat{\mathbf{H}}_h$ and $\hat{\mathbf{H}}_\theta$ without presenting, for the sake of coinciseness, those non-negligible transfer functions that are easily derivable by observing that λ_s vs C_L and C_M are fully equivalent (in hovering) to λ_c vs C_M and C_L.

As already observed in Ref. [10] for single rotors, the Pitt-Peters-type inflow model derived from $\mathbf{H}_\theta$ (*i.e.,* from $\mathbf{q}_\theta$ perturbations) is different from that obtained from $\mathbf{H}_h$ (*i.e.,* from $\mathbf{q}_h$ perturbations). This may be explained by noting that similar rotor loads are achievable by dif-

ferent distributions of blade sectional loads, and hence bound circulation which, in turn, implies different release of wake vorticity and corresponding induced velocity field.

However, it is interesting to note that for the coaxial rotor examined the most important transfer functions (*i.e.,* λ_0 vs C_T, λ_s vs C_L and hence λ_c vs C_M, see Figs. 6(a)-6(d)) derived from $\mathbf{q}_\theta$ and $\mathbf{q}_h$ are in much higher agreement than the corresponding ones evaluated for the single rotor case.[10] Different perturbations provide quite different transfer functions when considering cross-coupling effetcs (like, for instance, λ_s vs C_M, see Figs. 6(e) and 6(f)). This closer similarity between $\hat{\mathbf{H}}_\theta$ and $\hat{\mathbf{H}}_h$ is probably the beneficial effect of deriving the Pitt-Peters-type model from a larger set of inputs (6 instead of 3 for single rotors) which is representative of a larger domain of perturbed operative conditions and corresponding load distributions. This results suggests that, for single rotors, a Pitt-Peters-type model almost invariant with perturbation variables applied could be obtained by increasing the number of loads included.

(a) λ_0 vs θ_0^-.

(b) λ_0 vs θ_0^+.

(c) λ_s vs θ_c^-.

(d) λ_s vs θ_c^+.

(e) λ_s vs θ_s^-.

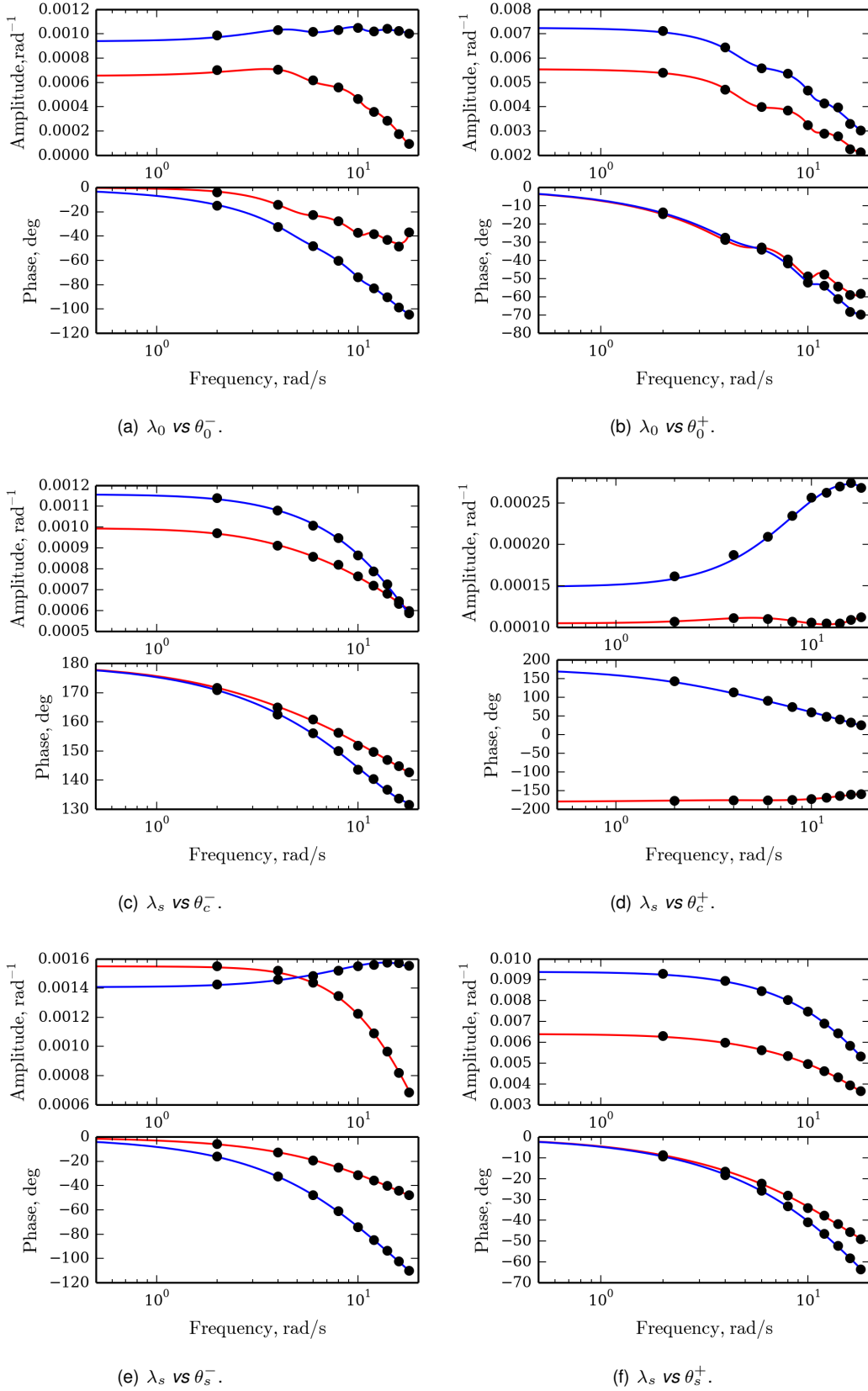(f) λ_s vs θ_s^+.

Figure 4: Transfer functions between blade pitch control variables and wake inflow coefficients, for upper (red) and lower (blue) rotor. Hovering condition. Solid lines=RMA; Bullets: sampled values.

(a) λ_0 *vs* w.

(b) λ_0 *vs* r.

(c) λ_s *vs* u.

(d) λ_s *vs* v.

(e) λ_s *vs* p.
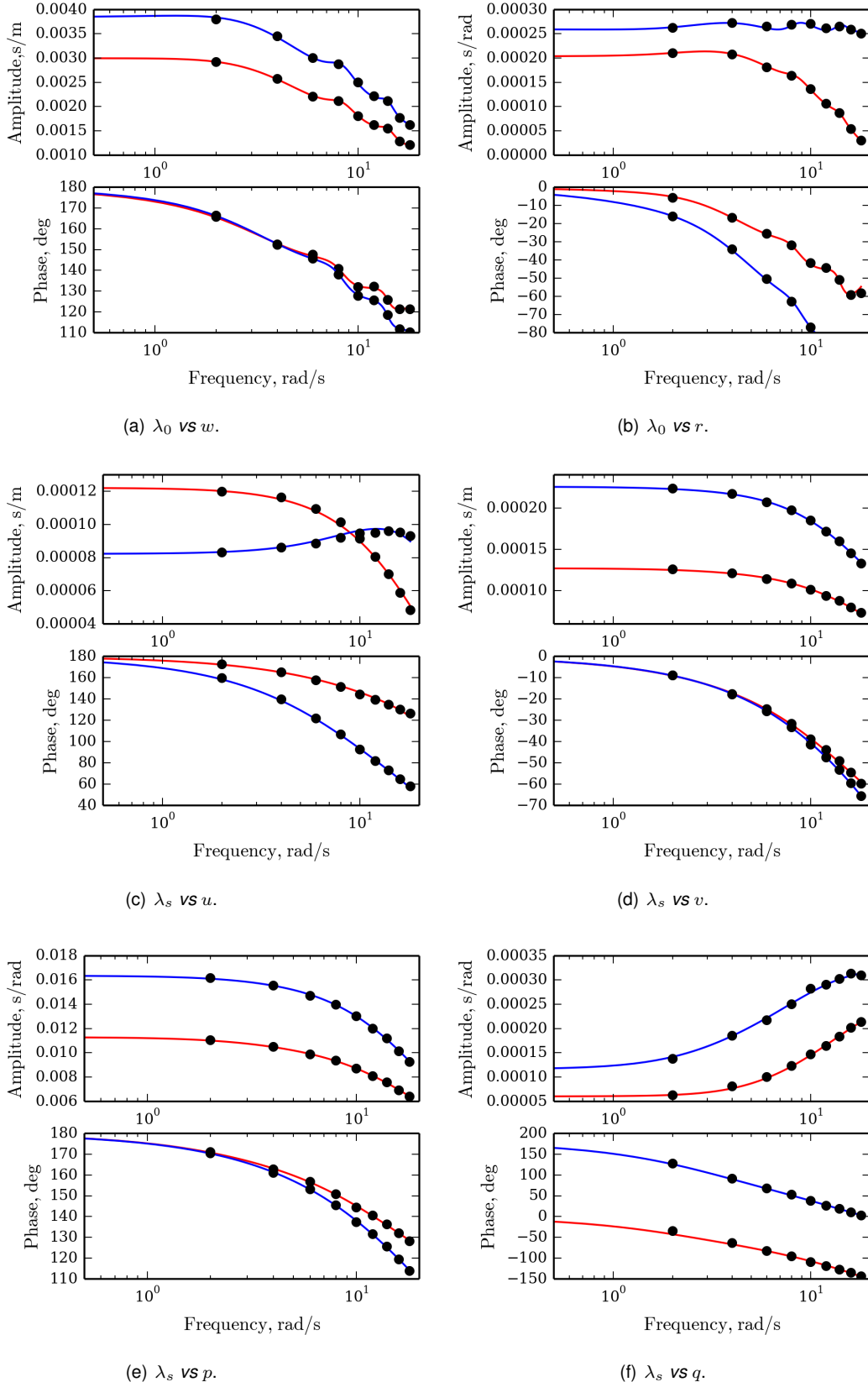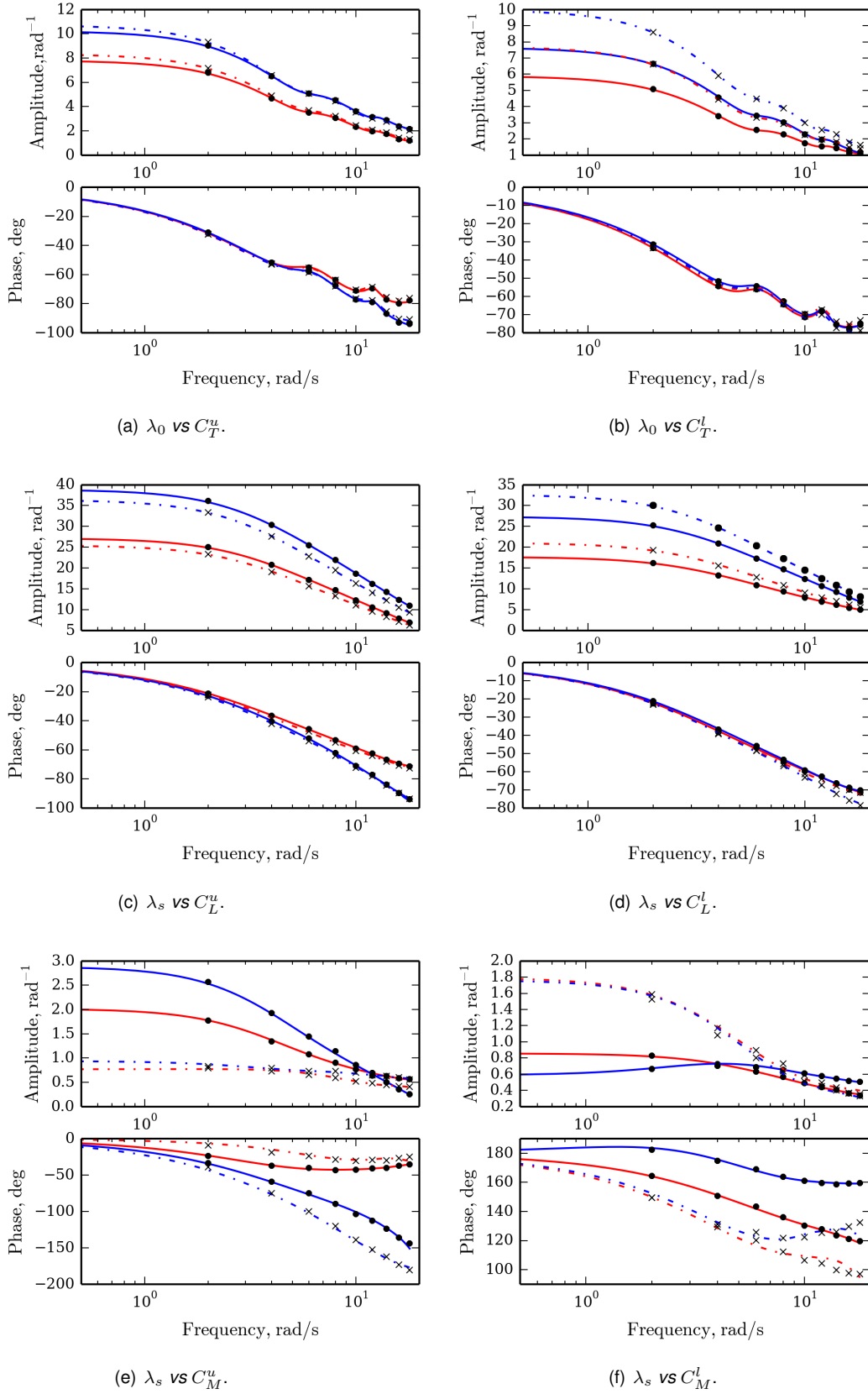
(f) λ_s *vs* q.

Figure 5: Transfer functions between kinematic variables and wake inflow coefficients, for upper (red) and lower (blue) rotor. Hovering condition. Solid lines=RMA; Bullets: sampled values.

(a) λ_0 *vs* C_T^u.

(b) λ_0 *vs* C_T^l.

(c) λ_s *vs* C_L^u.

(d) λ_s *vs* C_L^l.

(e) λ_s *vs* C_M^u.

(f) λ_s *vs* C_M^l.

Figure 6: Transfer functions of Pitt-Peters-type wake inflow model, for upper (red) and lower (blue) rotor. Hovering condition. Solid lines=RMA of $\hat{\mathbf{H}}_\theta$; Dashed lines: RMA of $\hat{\mathbf{H}}_h$; Bullets: sampled values of $\hat{\mathbf{H}}_\theta$; Crosses: sampled values of $\hat{\mathbf{H}}_h$.
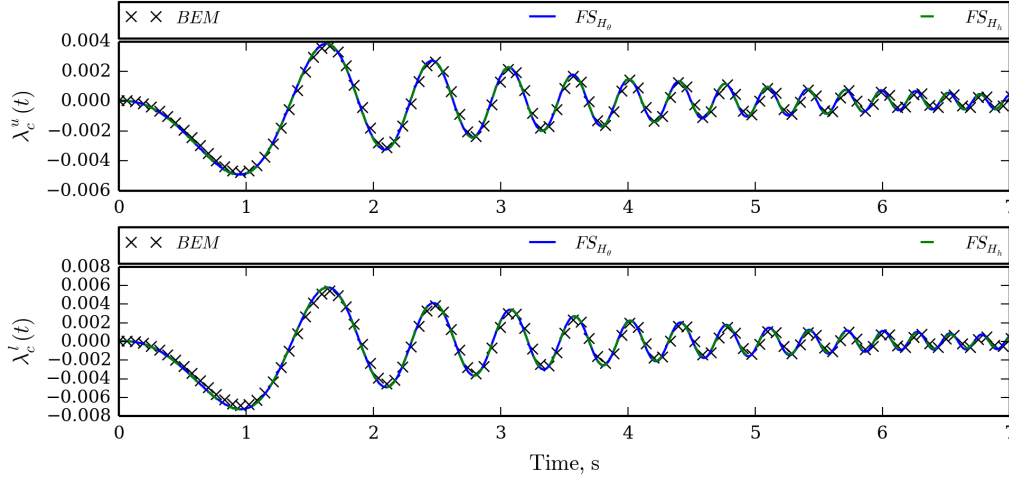
Figure 7: Time response of λ_c to θ_c^+ perturbation. Pitt-Peters-type finite-state (FS_{H_h}, FS_{H_θ}) *vs* BEM predictions.

From Fig. 6 the following general consideration may be drawn: i) the mutual influence between the two rotors is significant; ii) the influence of upper rotor loads on lower rotor inflow is higher than the influence of lower rotor loads on upper rotor inflow; iii) RMAs are of excellent quality for all of the transfer functions examined.

3.4. Time response validation of Pitt-Peters-type model for hovering rotor

Next, in order to assess the capability of the Pitt-Peters-type model proposed here to predict wake inflow perturbations, its outcomes deriving from arbitrary kinematic/pitch control variables inputs are compared with those directly given by the non-linear, time-marching aerodynamic BEM solver used for $\mathbf{H}_h$ and $\mathbf{H}_\theta$ sampling.

Considering, without loss of generality, the following arbitrary perturbation of blade cyclic pitch, θ_c^+, (expressed in degrees)

(8) $\theta_c^+(t) = \sin(3t^2)\, e^{-0.25t}$

first, the related perturbation wake inflow and rotor loads in hovering condition are determined by the BEM solver and then, the latter are used to force the LTI, Pitt-Peters-type, finite-state model. Figures 7 and 8 compare corresponding BEM and finite-state model predictions on upper and lower rotors of $\lambda_c(t)$ and $\lambda_s(t)$, respectively.

The results are shown for two different Pitt-Peters-type models, namely those obtained by $\mathbf{H}_v$ and $\mathbf{H}_\theta$. As expected from the accuracy of the transfer functions RMA

observed above, the predictions given by the finite-state model derived from $\mathbf{H}_\theta$ are in excellent agreement on both rotors, both for $\lambda_c(t)$ and $\lambda_s(t)$, with the BEM simulations. Indeed, in this case, only RMA inaccuracy and non-linearities (negligible, due to the small amplitude of the input) may give rise to discrepancies. Instead, when a Pitt-Peters-type model identified through variables different from those perturbing the rotor, coherently with the results shown in Fig. 6, the analytic solutions are not always in agreement with BEM's ones. Specifically, the Pitt-Peters-type model based on $\mathbf{H}_h$ is capable of capturing with very good accuracy $\lambda_c(t)$ responses on upper and lower rotor, whereas low-accuracy results are obtained for the simulation of $\lambda_s(t)$ responses (see Fig. 8).

However, it is interesting to note that the analysis of the rest of wake inflow coefficients and the application of different inputs, confirm that the most important wake inflow coefficients are predicted with similar good accuracy by both Pitt-Peters-type models; only the representation of terms of secondary importance reveal a strong dependence on the kind of perturbation variables the analytical model is derived from. This is an important improvement with respect to the results obtained for single rotor systems, for which the the kind of perturbation variables used to determine the Pitt-Peters-type model may strongly affect the accuracy of the predictions of significant wake inflow coefficients.

Finally, it is worth noting that the finite-state model based on kinematic inputs (see Eq. 2) provides time responses that are in almost perfect agreement with non-
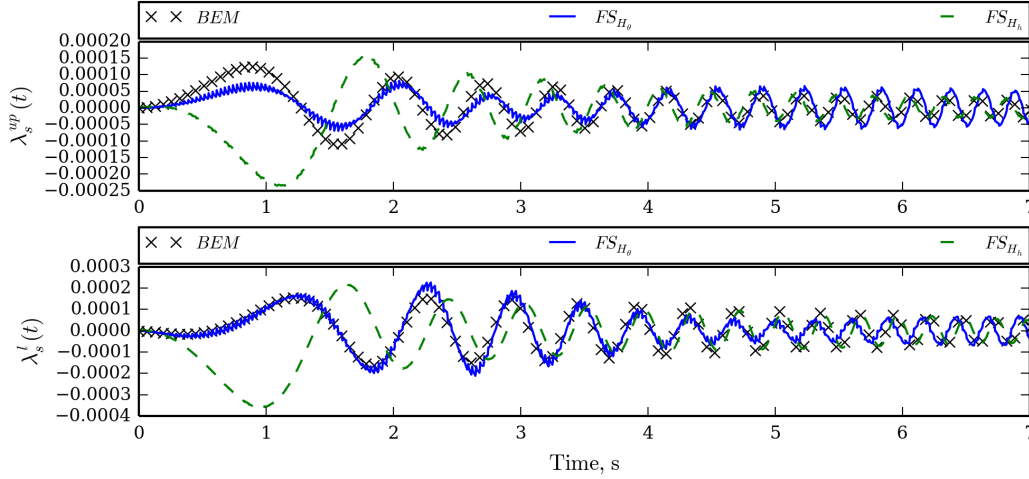
Figure 8: Time response of λ_s to θ_c^+ perturbation. Pitt-Peters-type finite-state (FS_{H_h}, FS_{H_θ}) *vs* BEM predictions.

linear BEM solutions, without exception on any inflow component.

3.5. Transfer functions of Pitt-Peters-type model for advancing rotor

Finally, in order to prove the capability of the proposed approach to determine finite-state wake inflow models for advancing rotors, Fig. 9 shows some of the most important transfer functions of the Pitt-Peters-type model derived from blade pitch perturbations, for $\mu = 0.2$.

It is interesting to observe that, in comparison with the equivalent transfer functions for hovering condition (see Fig. 6), lower coupling occurs between upper and lower rotors: indeed, in this case, upper/lower rotor load perturbations produce higher perturbations of upper/lower rotor wake inflow components, whereas Fig. 6 shows that lower rotor wake inflow perturbations are higher than upper rotor ones, independently on the perturbed load. Furthermore, it is confirmed that λ_s is strongly dependent on C_L perturbations and weakly dependent on C_M perturbations (the opposite occurs for λ_c).

Likewise the hovering rotor case, the RMA is of excellent accuracy, thus assuring the definition of accurate finite-state wake inflow modelling.

4. CONCLUSIONS

Finite-state modelling of wake inflow of coaxial rotors in arbitrary steady motion has been proposed. It is an extension to multiple-rotor systems of the methodology recently proposed by the authors for single rotor anal-

ysis. Two models concerning linear inflow approximations over the rotor disks have been presented: one relating upper and lower inflow coefficients with flight dynamics state variables and blade pitch controls, the other (Pitt-Peters-type) relating upper and lower inflow coefficients with thrust and in-plane moments (namely, rolling and pitching) generated by the two rotors. These models are determined through the rational approximation of the transfer functions involved which, in turn, are identified by a harmonic perturbation technique based on time-marching solutions provided by an aerodynamic solver, whose accuracy affects that of the resulting wake inflow model. The following conclusions are drawn from the numerical investigation:

– the applied RMA algorithm is able to identify with excellent accuracy the sampled transfer functions of wake inflow coefficients;

– in hovering conditions, the lower rotor wake inflow components have amplitude that is generally higher than upper rotors one, and have a slower decay with frequency increase, thus revealing the presence of high-frequency poles;

– the Pitt-Peters-type model (namely, the description of the wake inflow coefficients in terms of rotor loads) is not unique, but rather, it is dependent on the kinematic perturbation used to identify the model; however, this dependency is significantly reduced with respect to what is observed for single rotors: for the coaxial rotor operating condition examined, it seems to have strong effects only on the description of minor transfer functions coupling
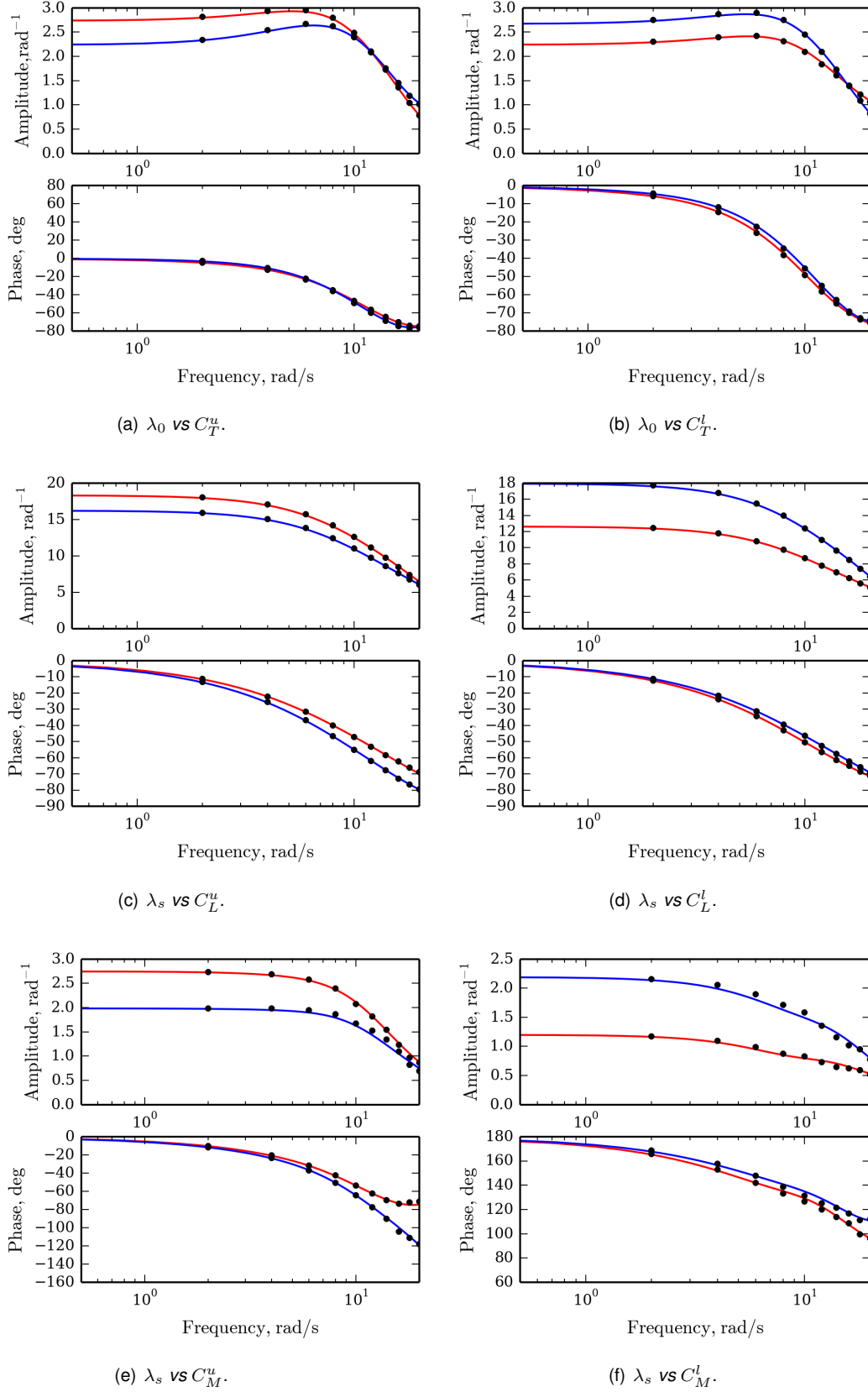
Figure 9: Transfer functions of Pitt-Peters-type wake inflow model, for upper (red) and lower (blue) rotor. Forward flight condition, $\mu = 0.2$. Solid lines=RMA of $\hat{\mathbf{H}}_\theta$; Bullets: sampled values of $\hat{\mathbf{H}}_\theta$.

lateral and longitudinal variables;

– the model is capable of capturing the effects of mutual influence occurring between the two rotors;

– the time histories of linear wake inflow approximation components corresponding to arbitrary rotor perturbations predicted by the proposed finite-state Pitt-Peters-type model is in very good agreement with those obtained by the time-marching BEM aerodynamic solver, with the exception of some minor longitudinal/lateral coupling terms; upper/lower rotor mutual influence is perfectly captured by the analytical model.

– the time responses predicted by the model based on kinematic inputs are in excellent agreement with BEM solutions for any small perturbation input, and wake inflow component.

The results presented in this paper have been obtained by a prescribed wake shape aerodynamic solution. This simplification has been motivated by the goal of the paper which is to demonstrate that the proposed methodology is feasible and capable of providing accurate finite-state wake inflow modelling for coaxial rotors. Next activity will include the determination of more realistic wake inflow models based on free-wake aerodynamic analyses.

REFERENCES

[1] S. J. Newman, "The compound helicopter configuration and the helicopter speed trap," *Aircraft Engineering and Aerospace Technology: An International Journal*, vol. 69, no. 5, pp. 407–413, 1997.

[2] A. J. Ruddell et al., "Advancing Blade Concept (ABC) Technology Demonstrator," *Tech. Rep. USAAVRADCOM-TR-81-D-5, Sikorsky Aircraft Division of United Technologies Corporation*, 1981.

[3] V. M. Paglino, "Forward Flight Performance of a Coaxial Rigid Rotor," *27th Annual National Forum of the American Helicopter Society*, no. Washington, D.C., May, 1971.

[4] P. P. Friedmann, "Rotary-Wing Aeroelasticity: Current Status and Future Trends," *AIAA Journal*, vol. 42, no. 10, pp. 1953–1972, 2004.

[5] J. G. Leishman, *Principles of helicopter aerodynamics*. Cambridge aerospace series, Cambridge, New York: Cambridge University Press, 2000.

[6] D. M. Pitt and D. A. Peters, "Theoretical Predictions of Dynamic Inflow Derivatives," *Vertica*, vol. 5, pp. 21–34, 1981.

[7] D. M. Pitt and D. A. Peters, "Rotor dynamic inflow derivatives and time constants from various inflow models," in *15th European Rotorcraft Forum: September 13-15, 1983, Stresa, Italy*, 1983.

[8] M. Gennaretti and L. Greco, "A time-dependent coefficient reduced-order model for unsteady aerodynamics of proprotors," *Journal of Aircraft*, vol. 42, no. 1, pp. 138–147, 2005.

[9] R. Gori, J. Serafini, M. Molica Colella, and M. Gennaretti, "Assessment of a state-space aeroelastic rotor model for rotorcraft dynamics analysis," *XXII Conference of the Italian Association of Aeronautics and Astronautics*, pp. 1–12, 2013.

[10] M. Gennaretti, R. Gori, J. Serafini, G. Bernardini, and F. Cardito, "Rotor Dynamic Wake Inflow Finite-State Modelling," *33rd AIAA Applied Aerodynamics Conference*, Dallas, TX, June 2015.

[11] M. Gennaretti and G. Bernardini, "Novel boundary integral formulation for blade-vortex interaction aerodynamics of helicopter rotors," *AIAA Journal*, vol. 45, no. 6, pp. 1169–1176, 2007.

[12] M. Gennaretti and D. Muro, "Multiblade reduced-order aerodynamics for state-space aeroelastic modeling of rotors," *Journal of Aircraft*, vol. 49, no. 2, pp. 495–502, 2012.

[13] J. Serafini, M. Molica Colella, and M. Gennaretti, "A finite-state aeroelastic model for rotorcraft-pilot coupling analysis," *CEAS Aeronautical Journal*, pp. 1–11, 2013.

[14] R. Gori, F. Pausilli, M. D. Pavel, and G. M, "State-space rotor aeroelastic modeling for real-time helicopter flight simulation," *Advanced Material Research*, vol. 1016, pp. 451–459, 2014.

[15] G. Bernardini, J. Serafini, S. Ianniello, and M. Gennaretti, "Assessment of computational models for the effect of aeroelasticity on bvi noise prediction," *International Journal of Aeroacoustics*, vol. 6, no. 3, pp. 199–222, 2007.

[16] M. Gennaretti, M. M. Colella, and G. Bernardini, "Prediction of tiltrotor vibratory loads with inclusion of wing-proprotor aerodynamic interaction," *Journal of Aircraft*, vol. 47, no. 1, pp. 71–79, 2010.